EPJ manuscript No.
(will be inserted by the editor)

Measurement of charged pions in ^{12}C + ^{12}C collisions at 1A GeV and 2A GeV with HADES

G. Agakishiev[8], C. Agodi[1], A. Balanda[3,V], G. Bellia[1,I], D. Belver[15], A. Belyaev[6], J. Bielcik[4], A. Blanco[2], A. Bortolotti[9]; J. L. Boyard[13], P. Braun-Munzinger[4], P. Cabanelas[15], S. Chernenko[6], T. Christ[11], R. Coniglione[1], M. Destefanis[8], J. Díaz[16], F. Dohrmann[5], I. Durán[15], A. Dybczak[3], T. Eberl[11], L. Fabbietti[11], O. Fateev[6], R. Ferreira-Marques[2,III], P. Finocchiaro[1], P. Fonte[2,II], J. Friese[11], I. Fröhlich[7], T. Galatyuk[4], J. A. Garzón[15], R. Gernhäuser[11], A. Gil[16], C. Gilardi[8], M. Golubeva[10], D. González-Díaz[4], E. Grosse[5], F. Guber[10], M. Heilmann[7], T. Heinz[4], T. Hennino[13], R. Holzmann[4], A. Ierusalimov[6], I. Iori[9,IV], A. Ivashkin[10], M. Jurkovic[11], B. Kämpfer[5], K. Kanaki[5], T. Karavicheva[10], D. Kirschner[8], I. Koenig[4], W. Koenig[4], B. W. Kolb[4], R. Kotte[5], A. Kozuch[3,V], A. Krása[14], F. Křížek[14], R. Krücken[11], W. Kühn[8], A. Kugler[14], A. Kurepin[10], J. Lamas-Valverde[15], S. Lang[4], J. S. Lange[8], K. Lapidus[10], L. Lopes[2], M. Lorenz[7], L. Maier[11], C. Maiolino[1], A. Mangiarotti[2], J. Marín[15], J. Markert[7], V. Metag[8], B. Michalska[9], J. Michel[7], E. Morinière[13], J. Mousa[12 a], M. Münch[4], C. Müntz[7], L. Naumann[5], R. Novotny[8], J. Otwinowski[3], Y. C. Pachmayer[7], M. Palka[4], Y. Parpottas[12], V. Pechenov[8], O. Pechenova[8], T. Pérez Cavalcanti[8], P. Piattelli[1], J. Pietraszko[4], V. Pospíšil[14], W. Przygoda[3,e], B. Ramstein[13], A. Reshetin[10], M. Roy-Stephan[13], A. Rustamov[4], A. Sadovsky[10], B. Sailer[11], P. Salabura[3], P. Sapienza[1], A. Schmah[11], C. Schroeder[4], E. Schwab[4], R.S. Simon[4], Yu.G. Sobolev[14], S. Spataro[8], B. Spruck[8], H. Ströbele[7], J. Stroth[7,4], C. Sturm[7], M. Sudol[13], A. Tarantola[7], K. Teilab[7], P. Tlustý[14 b], M. Traxler[4], R. Trebacz[3], H. Tsertos[12], V. Wagner[14], M. Weber[11], M. Wisniowski[3], T. Wojcik[3], J. Wüstenfeld[5], S. Yurevich[4], Y. Zanevsky[6], P. Zhou[5], P. Zumbruch[4]

[1] Istituto Nazionale di Fisica Nucleare - Laboratori Nazionali del Sud, 95125 Catania, Italy
[2] LIP-Laboratório de Instrumentação e Física Experimental de Partículas , 3004-516 Coimbra, Portugal
[3] Smoluchowski Institute of Physics, Jagiellonian University of Cracow, 30-059 Kraków, Poland
[4] GSI Helmholtzzentrum für Schwerionenforschung, 64291 Darmstadt, Germany
[5] Institut für Strahlenphysik, Forschungszentrum Dresden-Rossendorf, 01314 Dresden, Germany
[6] Joint Institute of Nuclear Research, 141980 Dubna, Russia
[7] Institut für Kernphysik, Johann Wolfgang Goethe-Universität, 60438 Frankfurt, Germany
[8] II. Physikalisches Institut, Justus Liebig Universität Giessen, 35392 Giessen, Germany
[9] Istituto Nazionale di Fisica Nucleare, Sezione di Milano, 20133 Milano, Italy
[10] Institute for Nuclear Research, Russian Academy of Science, 117312 Moscow, Russia
[11] Physik Department E12, Technische Universität München, 85748 München, Germany
[12] Department of Physics, University of Cyprus, 1678 Nicosia, Cyprus
[13] Institut de Physique Nucléaire (UMR 8608), CNRS/IN2P3 - Université Paris Sud, F-91406 Orsay Cedex, France
[14] Nuclear Physics Institute, Academy of Sciences of Czech Republic, 25068 Rez, Czech Republic
[15] Departamento de Física de Partículas, University of Santiago de Compostela, 15782 Santiago de Compostela, Spain
[16] Instituto de Física Corpuscular, Universidad de Valencia-CSIC, 46971 Valencia, Spain
[I] Also at Dipartimento di Fisica e Astronomia, Università di Catania, 95125 Catania, Italy
[II] Also at ISEC Coimbra, Coimbra, Portugal
[III] Also at Universidade de Coimbra, Coimbra, Portugal
[IV] Also at Dipartimento di Fisica, Università di Milano, 20133 Milano, Italy
[V] Also at Panstwowa Wyzsza Szkola Zawodowa , 33-300 Nowy Sacz, Poland

Received: May 18, 2009/ Revised version: May 18, 2009

Abstract. We present the results of a study of charged pion production in ^{12}C + ^{12}C collisions at incident beam energies of 1A GeV and 2A GeV using the HADES spectrometer at GSI. The main emphasis of the HADES program is on the dielectron signal from the early phase of the collision. Here, however, we discuss the data with respect to the emission of charged hadrons, specifically the production of $\pi^{\pm}$ mesons, which are related to neutral pions representing a dominant contribution to the dielectron yield. We have performed the first large-angular range measurement of the distribution of $\pi^{\pm}$ mesons for the ^{12}C + ^{12}C collision system covering a fairly large rapidity interval. The pion yields, transverse-mass and angular distributions are compared with calculations done within a transport model, as well as with existing data from other experiments. The anisotropy of pion production is systematically analyzed.

PACS. 25.75.-q heavy-ion collisions - 25.75.Dw charged pion spectra

1 Introduction

The investigation of nuclear matter at high temperature and high density is one of the major research topics in modern nuclear physics. Nucleus-nucleus collisions at relativistic energies offer the unique possibility to create such highly excited nuclear matter in the laboratory [1,2,3,4,5,6]. The study of particle production as function of beam energy, system size and centrality of the collisions has been instrumental in the past for understanding the approach of the system towards equilibrium and the generation of flow phenomena, as well as for gaining information about the nuclear equation of state. Collisions of the light ^{12}C + ^{12}C system represent a link between the elementary nucleon-nucleon reactions and the heavy-ion collisions of large nuclei. Important physics issues in this context are the degree of thermalization achieved, the role of the mean field and collective motion in such a small system.

In the few-GeV energy range, pions are the only abundantly produced mesons. In heavy-ion collisions their spectra and yields are affected by collective effects like thermalization, directed and elliptic flow, as well as by possible modifications of the properties of the baryon resonances they stem from, in particular the Δ [7,8]. The subtle interplay of the phenomena which change the characteristics of pion production with respect to nucleon-nucleon interactions is indeed a challenge to theoretical interpretations.

Best suited for a description of all phases of the complex dynamics of heavy-ion reactions are transport models, based on microscopic kinetic theory. The reaction is simulated as a network of multiple elementary collisions optionally embedded in a mean field equipped with momentum-dependent potentials. These assumptions are then tested by comparing the experimental observables with the model predictions and allow to an understanding of the reaction dynamics. Transport models achieve a remarkable success in describing bulk properties of the interactions over a large energy and system size scale (cf. [1, 2,3,4,5,6]). At the same time, however, for special channels, problems are met in reproducing precisely the experimental data. For a recent comprehensive discussion of various differential pion observables and their comparison with model calculations in the region of 1A GeV see [9].

The High Acceptance DiElectron Spectrometer (HADES) [10], in operation at the heavy-ion synchrotron SIS18 at GSI, Darmstadt, is designed for high-resolution and high-acceptance dielectron spectroscopy in hadron-hadron, hadron-nucleus, and nucleus-nucleus reactions at beam energies in the range from 1A GeV to 2A GeV. Being a charged-particle detector, it is of course also an efficient device for hadron detection. First results from HADES on dielectron production in ^{12}C + ^{12}C reactions have been presented in [11,12]. The interpretation of the dilepton spectra relies on a precise knowledge of the differential yields of neutral pions which are the source of the bulk of the detected dielectron pairs, namely via the π^0 Dalitz and photon decays. In these analyses, the π^0 yields were inferred from the charged-pion yields measured by HADES in the same ^{12}C + ^{12}C data samples.

In this paper we present detailed data on charged pions obtained from ^{12}C + ^{12}C collisions at 1A GeV and 2A GeV. For the first time, large intervals of rapidity ($\approx \pm 0.8$ in y/y_{beam} for 2A GeV) and of centre-of-mass angle ($-0.7 < \cos(\theta_{cms}) < 0.7$) are covered. Our results are compared to UrQMD transport-model predictions and experimental data from other experiments.

2 Experiment

HADES [10] is a magnetic spectrometer designed as second-generation device for measurements of e^+e^- pairs. The spectrometer, schematically depicted in Fig. 1, is segmented into six identical sectors that cover laboratory polar angles between 18 and 85 degrees. Its large azimuthal acceptance covers between 65% and 90% of 2π at small and large polar angles, respectively. The analysis of charged pions presented here is based on the same setup as used in the lepton analyses of [11,12]. A fast hadron-blind Ring Imaging CHerenkov counter (RICH) is used for electron and positron identification. In the pion analysis, the RICH information was not used. Four planes of Multi-wire Drift Chambers (MDC I - MDC IV), together with a superconducting magnet, form the magnetic spectrometer for track reconstruction and momentum determination. In the region behind the magnetic field, a set of electromagnetic Pre-Shower detectors (at polar angles $18^\circ - 45^\circ$) [13] and a time-of-flight wall [14] are installed which form the META (Multiplicity and Electron Trigger Array). The time-of-flight detector wall is subdivided into 2 regions: TOF (at polar angles $45^\circ - 85^\circ$), consisting of 384 scintillator slabs of varying length, which are read out at both ends, with a time-of-flight resolution of $\sigma = 150$ ps, and TOFINO (at polar angles $18^\circ - 45^\circ$), consisting of 24 scintillator plates readout on one end, with a time-of-flight resolution of $\sigma = 450$ ps. The TOFINO is placed directly in front of the Pre-Shower detector, which provides precise position measurement. The TOF/TOFINO detectors are also used for fast charged-particle multiplicity measurements. Together with the Pre-Shower detectors they provide additional lepton/hadron discrimination power and track coordinate measurements with a spatial resolution in the range from 14 to 25 mm.

A fast data acquisition system is used together with a two-level trigger scheme [15,16]: (a) LVL1 is based on a fast determination of the charged-particle multiplicity (M_{ch}) in the time-of-flight detectors. (b) LVL2 is based on a real time identification of electron and positron candidates. All LVL2-triggered events were written to tape, as well as a part of LVL1 (regardless of the LVL2 decision) events (typically 10%) for normalization purposes, hadron analysis and monitoring of the trigger performance. For the analysis presented here, only LVL1-triggered events were processed.

In the very first HADES physics run, the detector was operated using only the following sub-systems: the RICH, the two inner MDC planes, and the META, i.e. the two

[a] e-mail: mousa@ucy.ac.cy
[b] e-mail: tlusty@ujf.cas.cz

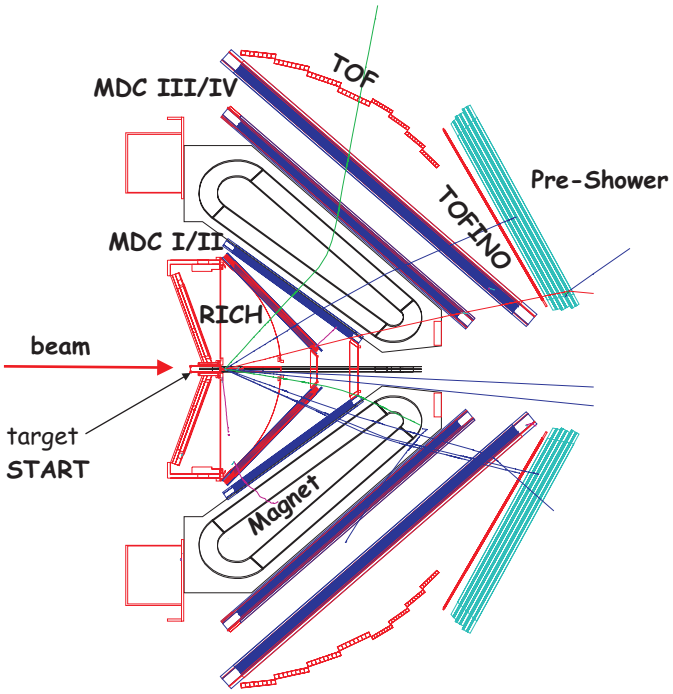

Fig. 1. Cut through two sectors of the HADES spectrometer. The magnet coils are projected onto the cut plane to visualize the toroidal magnetic field. The average distance between the target and the outermost detectors is about 210 cm.

outer MDC planes were not operational and the position measurements from the META were used for tracking. In this mode, the collision system ^{12}C + ^{12}C at 2A GeV was studied with a beam intensity of $I_{beam} = 10^6$ particles/sec impinging on a two-fold segmented carbon target with thickness of 2·2.5% interaction length. $1.67{\cdot}10^7$ LVL1 triggered events with $M_{ch} \geq 4$ were analyzed in this study. In the event reconstruction, the track segments measured in the two inner MDC planes were correlated with hits in the META.

In the second data taking period the ^{12}C + ^{12}C system was studied at 1A GeV. Then, for the first time, a high-resolution tracking mode exploiting also the outer MDC planes was available. In this measurement, a carbon beam of 10^6 particles/sec was focused onto a carbon foil of 3.8% interaction length. $1.62 \cdot 10^7$ LVL1-triggered events with $M_{ch} \geq 4$ were used in this analysis.

3 Data Analysis

3.1 Simulations

Artificial ^{12}C + ^{12}C events were generated with the UrQMD (v1.3b) transport code [17,18]. The detector response was simulated with the help of a GEANT 3.21 based package [19] including the geometry and characteristics of all HADES detectors. Then the same LVL1 trigger condition ($M_{ch} \geq 4$) was applied. The resulting raw data were processed in exactly the same way as the real data and used for efficiency corrections as well as to estimate systematic errors. Details on the different procedures are given in the corresponding subsections. For 1A GeV we have analyzed $2.14 \cdot 10^7$ (LVL1) UrQMD events, for 2A GeV $2.07 \cdot 10^7$ events, i.e. numbers being comparable to the amount of analyzed real data. For this sample size, the statistical errors of the π yields in the region of interest are negligible. Systematic errors are not addressed by the UrQMD itself, but may be elucidated by comparison with data. For the description of the apparently complex process of pion production in heavy-ion reactions in this energy range, the precision of transport models is not expected to be better than 20% [4].

Additionally, we simulated the π meson emission using a simple Monte-Carlo event generator PLUTO [20], which assumes a thermal source modified by a polar angular distribution. The simulation parameters used for PLUTO - inverse slopes and anisotropies - were derived from our measured data. The generated rapidity distribution has been used to extrapolate the pion yields outside our detector acceptance. Varying the input parameters of the generator within their errors provides estimates for the systematic error of the extrapolation.

3.2 Momentum reconstruction

When traversing the spectrometer, charged particles are deflected in the magnetic field and at the same time they leave "hits" in the MDCs and META detectors. From this information, together with the known magnetic field, their trajectories are reconstructed and their momenta are deduced.

Two different tracking methods have been developed and were both used in the present analysis (see [10] for details). The first one is the "kickplane" algorithm which uses the position information delivered by the inner MDC chambers and the META system. In this case the momentum resolution σ_p/p, dominated by the limited position resolution of META, has been determined in simulations to be $\simeq 2.5\%$ at a momentum of 150 MeV/c, with a linear increase up to 16% at 1400 MeV/c, with a weak dependence on polar angle. The second method is based on a Runge-Kutta trajectory integration routine [21] which uses the information from all four MDC planes, resulting in a resolution $\sigma_p/p \simeq 1.8\%$ at 150 MeV/c and $\simeq 4.3\%$ at 1400 MeV/c. To obtain the results presented in this paper, the kickplane method has been applied to the 2A GeV data, and both methods were used and compared for the 1A GeV data.

3.3 Particle identification

Particle identification in the HADES data analysis (for details see [10]) is based on Bayesian statistics [22,23]. The method allows to evaluate the probability that the reconstructed track can be related to a certain particle species

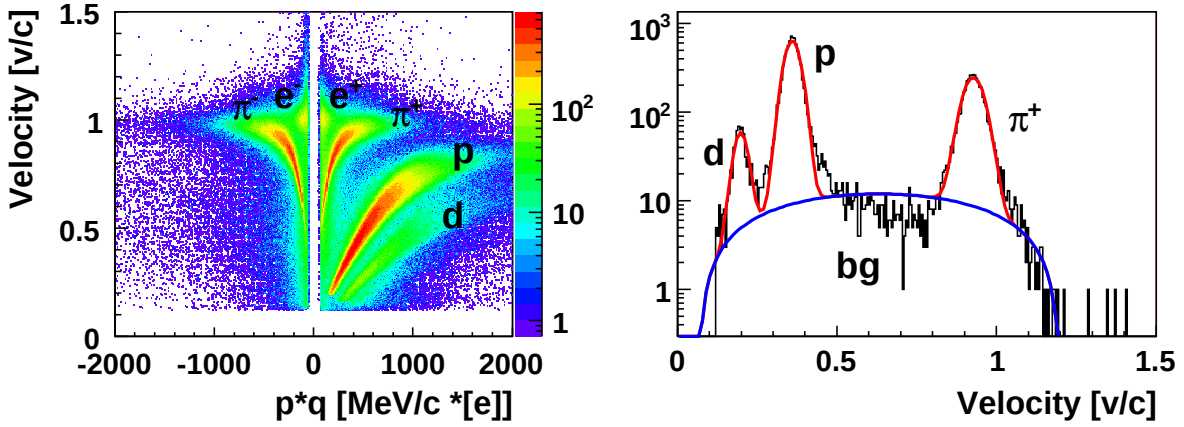

Fig. 2. Velocity vs. charge-times-momentum of charged particles as seen by the HADES detector from ^{12}C + ^{12}C collisions at 2A GeV (left). Projection onto the velocity axis of positively charged particles with momenta 350±5 MeV/c and $\theta = 60° \pm 5°$ (right). Fitted signal and background distributions are shown as lines.

(e.g. proton, kaon, pion, electron, etc.). It combines several observables from various sub-detectors (e.g. time-of-flight, energy loss) via probability density functions (PDF) determined for each observable and for all possible particle species. The probabilities for different mass assignments of any given track are calculated from the assumed abundances of the individual particle species and from the PDFs of all measured variables. The latter ones are obtained from simulations. If the assumed abundances differ significantly from the final results, the procedure is repeated with updated input distributions. It converges typically after one or two iterations. The performance of the method in terms of efficiency and purity is evaluated in detailed simulations and simultaneous comparisons with the real data. In our case, hadron identification has been performed using measured momenta and corresponding velocities computed by means of the time-of-flight. For more sophisticated analyses, like electron or rare-hadron identification, data from the RICH and PreShower detectors as well as the energy loss in META and MDCs can be used in addition.

The method used for Particle IDentification (PID) is illustrated in Fig. 2 for the case of particle velocity (right) deduced from the measured time-of-flight and track length ("velocity-vs-momentum" algorithm). Particles with different mass occupy different regions in the velocity-vs-momentum distribution (left side); the pronounced ridges correspond to positively and negatively charged pions, protons and deuterons. The very rare kaons are not visible in this representation. The Bayesian PID method requires the determination of the probability density functions for each particle species. In the case of the velocity-vs-momentum algorithm used here, the PDF is the probability distribution of velocity. For each type of particle it has been determined in bins of momentum and polar angle. In those velocity distributions Gaussian fits were used to obtain the signal (i.e. particle yields) and a 2^{nd}-order polynomial fit to obtain the background (due to fake tracks). The fitted distributions were normalized to unity. Fig. 2 (right side) shows as an example such a fit for the momentum bin 350±5 MeV/c in the polar angle range $\theta = 60° \pm 5°$.

Two quality parameters are used to characterize the performance of the method [24]: the PID efficiency and the PID purity. The PID efficiency $\varepsilon_t(p,\theta)$ is the probability that a particle with the true type t is identified as type t. The PID purity $\pi_t(p,\theta)$ is the probability that a particle that is identified as type t is truly of type t. The PID efficiency and purity have been studied in detailed simulations with events generated with the UrQMD model. The critical parameter here is the time resolution, which is however well known. Because of the moderate time resolution of the presently installed TOFINO detectors this limits the region in which we can use the method for π^+ and p identification to momenta < 1000 MeV/c . Finally, we have checked that varying particle abundances by a factor as large as 2 does not change the results significantly.

3.4 Total correction

Fig. 3 shows the dependencies of the PID efficiency and purity on momentum for π^+, π^- and protons for the 2A GeV data in the TOFINO (right) and TOF (left) region. The efficiency of pion and proton identification is larger than 95% for all momenta in the TOF region. In the TOFINO region, with its reduced time resolution, the efficiency to identify positively charged pions drops steeply above 1000 MeV/c due to the ambiguity with the protons. The purity of pions (lower plots) does not reach unity mainly because part of the tracks identified as pions are muons from in-flight pion decays. The strong contamination of the positively charged pions with protons for momenta above 1000 MeV/c is again due to the low time resolution of the TOFINO.

After the particle identification is done for all tracks, the resulting yields are corrected for efficiency and pu-

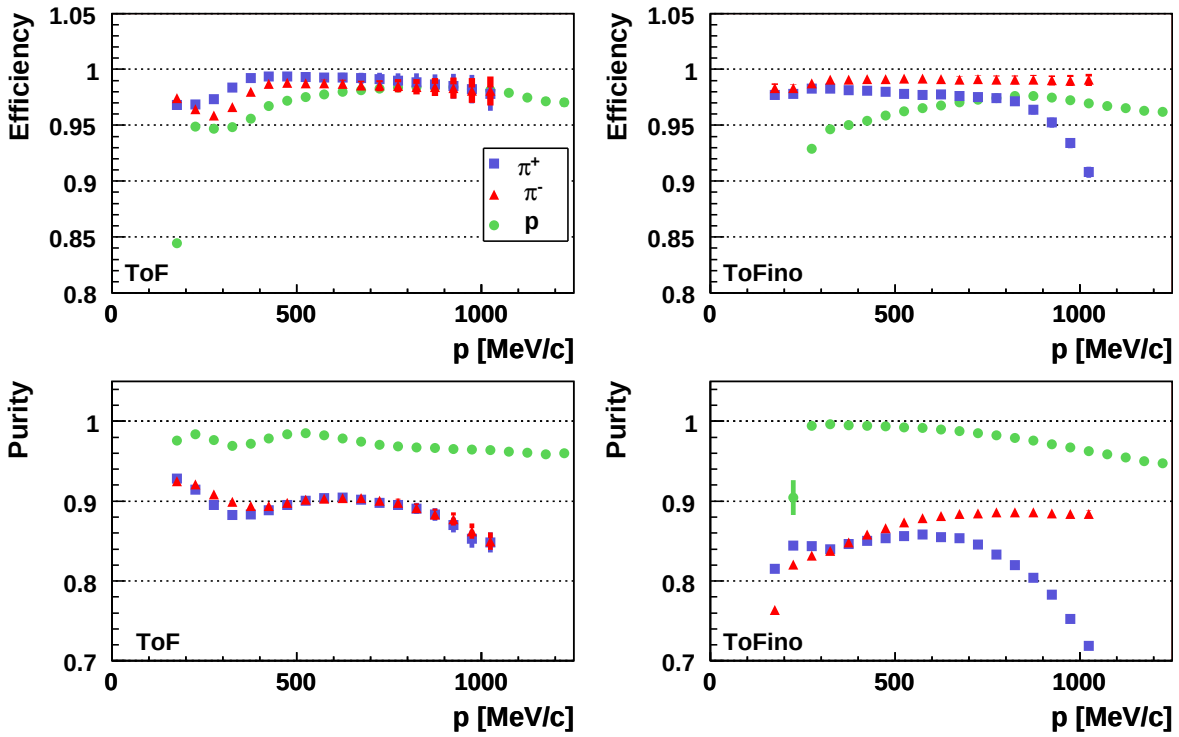

Fig. 3. Efficiency (top) and purity (bottom) of the PID method versus momentum for $\pi^{\pm}$ and protons in two sub-systems of the HADES detector: TOF (left) and TOFINO+PreShower (right) by using the kickplane reconstruction algorithm in ^{12}C + ^{12}C collisions at 2A GeV.

rity of the PID method, as well as for the detector and tracking efficiencies. The detection/tracking efficiency has also been obtained from Monte Carlo simulated and reconstructed UrQMD events. The reliability of the simulation was cross checked with real data by comparing and matching the information from different detectors and by selecting clean samples of (elastic) elementary collisions in which the track configurations can be obtained from the trigger detector (META) information only [10]. Using this information, realistic parameters were validated for the simulation.

The total correction applied to the reconstructed particle yields reads

$$w_t(p,\theta) = \frac{\pi_t(p,\theta)}{\varepsilon_t(p,\theta)\ \varepsilon_t^{det}(p,\theta)}, \qquad (1)$$

where $\varepsilon_t^{det}(p,\theta)$, the detection efficiency, subsumes detector, track reconstruction and acceptance losses. It should be noted that we specify $\varepsilon_t^{det}(p,\theta)$ as function of θ and p, while averaging over the azimuthal angle. In this way, corrections for missing geometrical acceptance at some azimuthal angles (namely the spaces occupied by the six magnet coils) are accounted for as well as the losses due to pion in-flight decays.

Figure 4 shows the dependence of the detection efficiency for $\pi^{\pm}$ and p as a function of momentum. The difference between proton and π efficiencies is again in part caused by the $\pi^{\pm}$ in-flight decay.

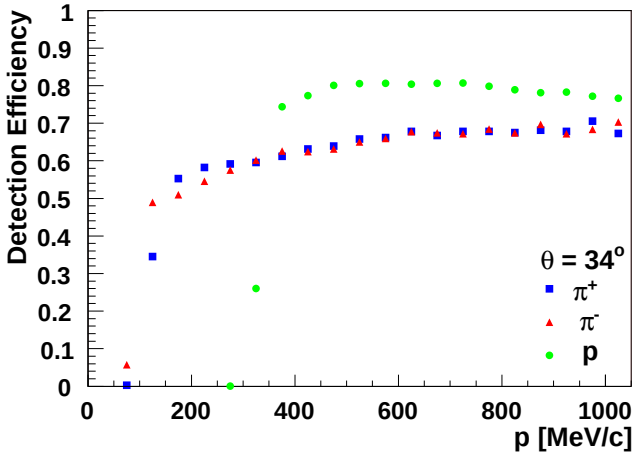

Fig. 4. The detection efficiency $\varepsilon_t^{det}(p,\theta)$ vs. momentum for $\pi^{\pm}$ and protons using the kickplane reconstruction in ^{12}C+^{12}C collisions at 2A GeV.

The total correction is applied to the data for each momentum and polar angle bin, and for each individual particle species. This is done only for bins with sufficiently high efficiency $\varepsilon_t^{det}(p,\theta) > 0.35$ in order to avoid large corrections at the sector boundaries. Data outside of this fiducial volume were excluded from further analysis.

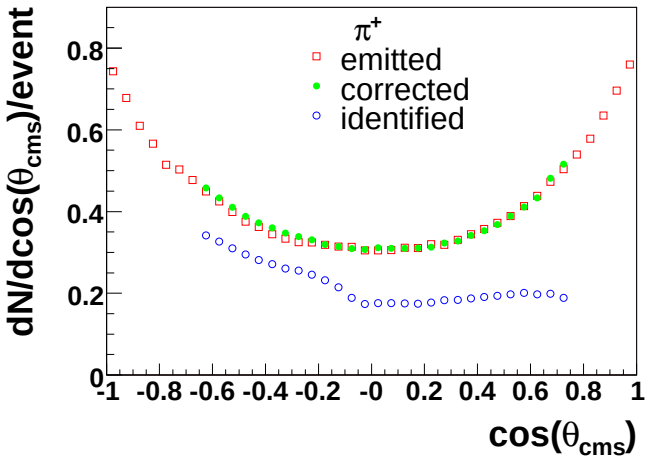

Fig. 5. Center-of-mass polar angle distributions of π^+. The squares represent the pions as generated by UrQMD. Only π mesons with $p_{cms} > 200$ MeV/c have been selected. The open circles show those generated pions which are detected and identified in the HADES acceptance. The full circles depict the result of the efficiency and purity correction to the accepted simulated pions.

Figure 5 presents simulated polar distributions of pions in the center-of-mass system (cms). It shows the identified π^+ before and after applying the total correction, together with the primordial distribution delivered by the UrQMD model for 2A GeV ^{12}C + ^{12}C collisions. This self-consistency check quantifies $w_t(p,\theta)$ as a function of $\cos\theta_{cms}$ and demonstrates the wide coverage of our spectrometer. In Fig. 5 the angular anisotropy of pion emission in the UrQMD model is clearly visible.

The point-to-point systematic errors of the measured distributions stem mainly from imperfect modelling of the detectors, reconstruction and identification efficiency. They are estimated as $\approx 5\%$, based on a comparison of measurements in the six independent HADES sectors. It should be noted that although the six sectors are identical in design, they are different at small scales like malfunction of electronic channels and small mechanical displacements. The resulting errors are of statistical nature and thus appropriate for fits to the various distributions. The geometry of the chambers and the magnetic field measurement have some influence on high resolution tracking, but do not affect continuum distributions as those discussed in this work.

3.5 Event selection

For the present analysis, we used the HADES LVL1-triggered events, which are characterized by a hit multiplicity $M_{ch} \geq 4$ in the time-of-flight detectors. The correlation between the LVL1 trigger condition and the centrality of the reaction has been studied in Monte-Carlo simulations using the UrQMD and GEANT codes. Fig. 6 shows the simulated impact-parameter distributions. For the "minimum bias" events corresponding to the total reaction cross section we require in UrQMD at least one nuclear interaction (distribution marked by circles in Fig. 6). Then we pass these events through our analysis code and require that they fulfill the LVL1 condition (triangles in Fig. 6). We found that the LVL1-triggered events correspond to 52% and 60% of the total reaction cross section in ^{12}C + ^{12}C collisions at 1A GeV and 2A GeV, respectively. To extract the average number of participants for our trigger-biased events we proceeded in the following way: For minimum-bias events the average number of participating nucleons was estimated from a geometrical model [25], namely $\langle A_{part}^{m.b.}\rangle = A/2 = 6$. For reactions accepted by LVL1 we deduce the mean $\langle A_{part}\rangle$ by comparing the pion multiplicity of UrQMD for LVL1-accepted events to the one of minimum-bias events, using $\langle A_{part}\rangle$ scaling of pion production (see e.g. figure 32 in [2]), i.e. $\langle A_{part}\rangle = 6 \cdot \langle M_\pi^{LVL1}\rangle / \langle M_\pi^{min.b.}\rangle$. The LVL1 trigger effect is significant, and the number of participants increases by $\approx 40\%$. The average impact parameters, the average pion multiplicities and average number of participants from UrQMD are listed in Table 1 for true minimum-bias events and after applying the LVL1 trigger.

Table 1. Average impact parameters, pion multiplicities, and average number of participating nucleons from UrQMD calculations for ^{12}C + ^{12}C at 1A GeV and 2A GeV before and after applying the LVL1 trigger condition.

Beam energy = 1A GeV				
	$\langle b\rangle$	$\langle M_{\pi^+}\rangle$	$\langle M_{\pi^-}\rangle$	$\langle A_{part}\rangle$
minimum-bias events	3.95 fm	0.36	0.36	6
LVL1-triggered	3.01 fm	0.51	0.52	8.61
Beam energy = 2A GeV				
	$\langle b\rangle$	$\langle M_{\pi^+}\rangle$	$\langle M_{\pi^-}\rangle$	$\langle A_{part}\rangle$
minimum-bias events	3.95 fm	0.83	0.83	6
LVL1-triggered	3.18 fm	1.15	1.17	8.38

The distributions of the number of reconstructed tracks per LVL1 event of data and UrQMD simulations are in reasonable agreement, as shown in Fig. 7. This is a confirmation that the modelling of the detector and tracking efficiency as well as of the LVL1 event selection in our simulation is realistic. From the differences of the measured and simulated distributions of the number of charged hits in META and the number of reconstructed tracks we estimate a systematic error for the mean number of participants determined above, resulting in $\langle A_{part}\rangle = 8.61 \pm 0.60$ and $8.38^{+1.17}_{-0}$ for 1A GeV and 2A GeV, respectively.

Comparing the pion momenta and angular distributions for minimum-bias and LVL1 UrQMD events is an important check for how the trigger condition used in the experiment influences the measured spectra. We do not observe significant deviations between the two data sets, e.g. for the transverse mass distribution, the difference in the inverse slopes (see Section 4.1) is less than 1 MeV, and the A_2 parameters of the polar angle distributions

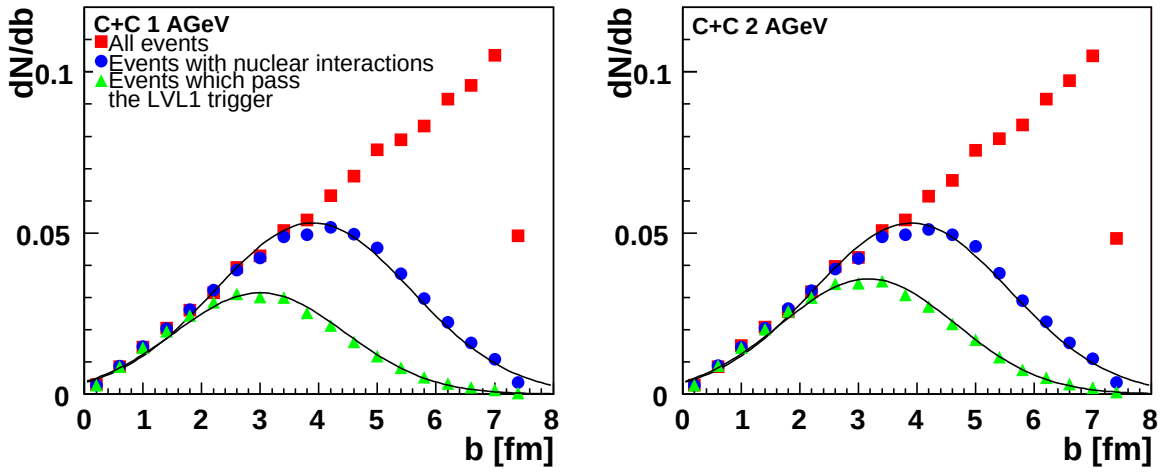

Fig. 6. The impact parameter distribution obtained from the UrQMD model for ^{12}C + ^{12}C collisions at 1 (left) and 2A GeV (right).

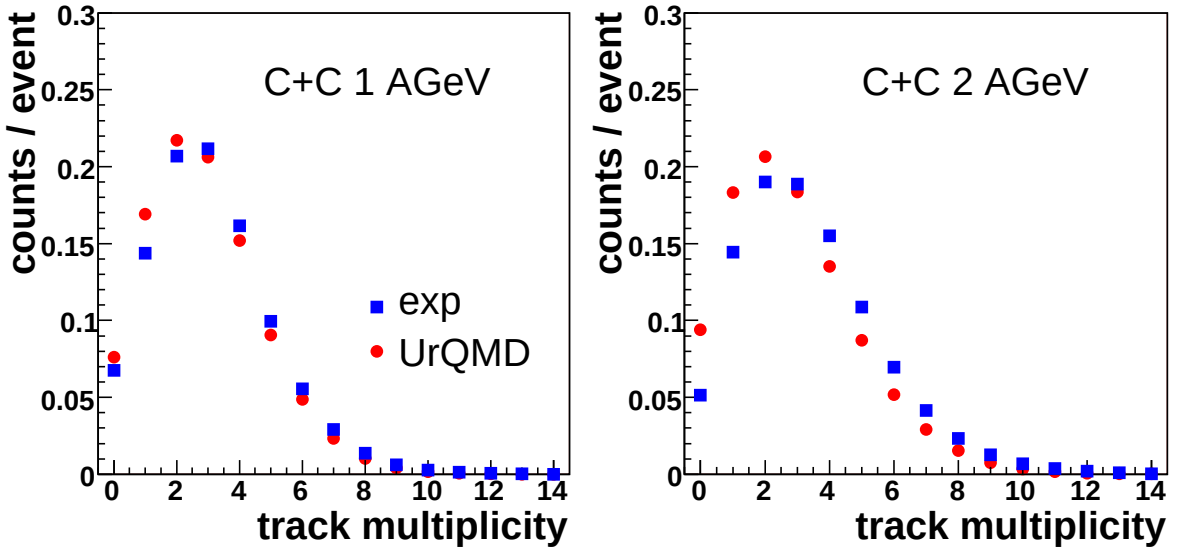

Fig. 7. Distribution of the number of reconstructed tracks in the data and in the simulation for 1A (left) and 2A GeV (right) ^{12}C + ^{12}C collisions.

(see Section 4.4) differ by less than 10%, while their momentum dependencies are identical. The reason is that for a small system such as ^{12}C + ^{12}C it is basically impossible to select events with well defined centrality by a charged-particle multiplicity trigger. This fact is clearly seen in Fig. 6, which shows a very broad distribution in impact parameter from the LVL1 events.

4 Results

4.1 Transverse-mass distributions

Figures 8 and 9 exhibit the measured and simulated transverse mass distributions of π^+ and π^- in different intervals of normalized rapidity $y_0 = (y_{lab} - y_{cms})/y_{cms}$ for ^{12}C + ^{12}C at 1A GeV and 2A GeV, respectively. The systematic errors of the data are estimated from point-to-point differences between distributions from the six independent HADES sectors as $\approx 5\%$ (see Sect. 3.5).

The transverse-mass ($m_\perp$) distributions have been fitted for each rapidity bin using one or two exponential functions. The fit with two slopes employs

$$\frac{1}{m_\perp^2}\frac{dN(y)}{dm_\perp} = C_1(y)\,\exp\left(-\frac{m_\perp}{T_1(y)}\right) + C_2(y)\,\exp\left(-\frac{m_\perp}{T_2(y)}\right) \quad (2)$$

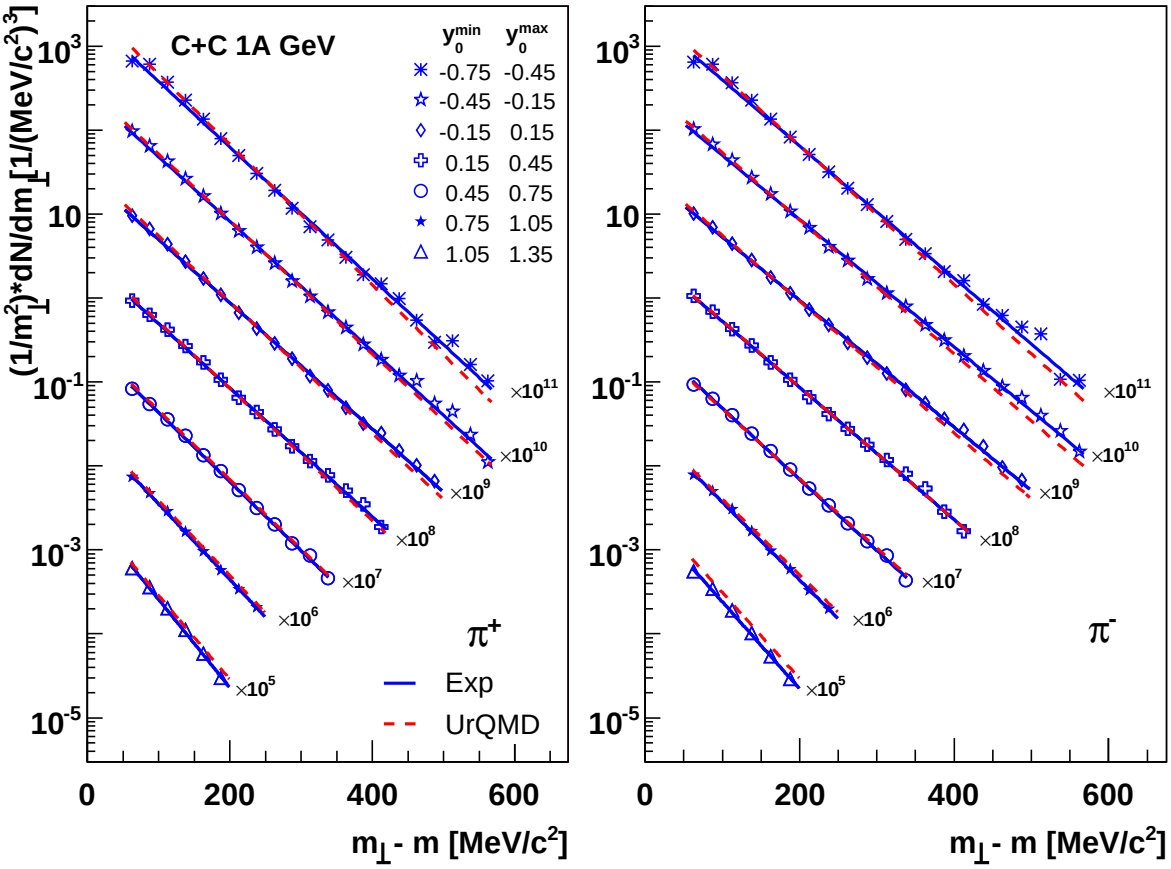

Fig. 8. Transverse-mass distributions for positively (left) and negatively (right) charged pions in different slices of rapidity derived from the data in ^{12}C + ^{12}C collisions at 1A GeV (LVL1 "semicentral" events). Full lines show the results of fits to the data (symbols) using one exponential function, while dashed lines show fits of the UrQMD distributions using the same fit function. Error bars (systematic and statistical ones) are not visible at this scale. Both data and UrQMD distributions are normalized to the number of LVL1 events.

with $m_\perp = (p_\perp^2 + m^2)^{1/2}$, and $p_\perp$ as transverse momentum. $C_{1,2}$ are normalizations and $T_{1,2}$ the inverse slope parameters; these parameters depend of course on rapidity. For the 2A GeV data, the two-component fit describes the experimental data better than a fit with one slope only (i.e., $C_2 \equiv 0$). For example, for the data at midrapidity χ^2/ndf is ≈ 1.0 as compared to 4.8 for the fit with one slope.

Figure 8 clearly demonstrates that for the lower bombarding energy of 1A GeV, a fit with one slope is sufficient for the description of the spectral shape. The inverse-slope parameters for π mesons at midrapidity for 1A GeV ($-0.15 \leq y_0 \leq 0.15$) and 2A GeV ($-0.1 \leq y_0 \leq 0.1$) are summarized in Table 2 using one or two exponential functions. The slopes of π^+ and π^- agree within error bars for the single exponential fit. At 2A GeV, UrQMD predicts different spectral shapes (purely exponential as compared to the concave shape of the real data), while at 1A GeV the agreement of UrQMD with data is better. Note that the errors of the fitted parameters are much larger in the case of two-slope fits than for the single exponential fits. The reason is occurrence of large correlations between the fit parameters in the two-slope case, which cause a considerable increase of the errors.

Thanks to the wide acceptance of the present experiment we can directly compare the data with results of previous experiments on charged pion production in ^{12}C + ^{12}C collisions at 1A GeV and 2A GeV done by the KaoS collaboration [26], and for neutral pions at 1A GeV and 2A GeV obtained by the TAPS collaboration [27]. For this purpose our data were passed through the respective acceptance filter of the previous measurements: $\pm 4^o$ around the laboratory polar angles θ_{lab} of the KaoS setup, and $0.42 < y_{lab} < 0.74$ and $0.80 < y_{lab} < 1.08$ for 1A GeV and 2A GeV, respectively, for the TAPS case. Then we rescaled the multiplicity per one LVL1 event to the minimum-bias cross section. For this we used a total reaction cross section of 0.95 b (calculated according to $\pi r_0^2 (A_p^{1/3} + A_t^{1/3})^2$, assuming $r_0 = 1.20$ fm) and the ratio of $\langle A_{part} \rangle$ for minimum-bias and LVL1 events from Table 1. Fig. 10 shows a comparison of our pion transverse-mass and momentum distributions with those of the TAPS and KaoS experiments, respectively. The TAPS data are shown both in linear and logarithmic scale to facilitate the comparison of yields as well as of spectral shapes.

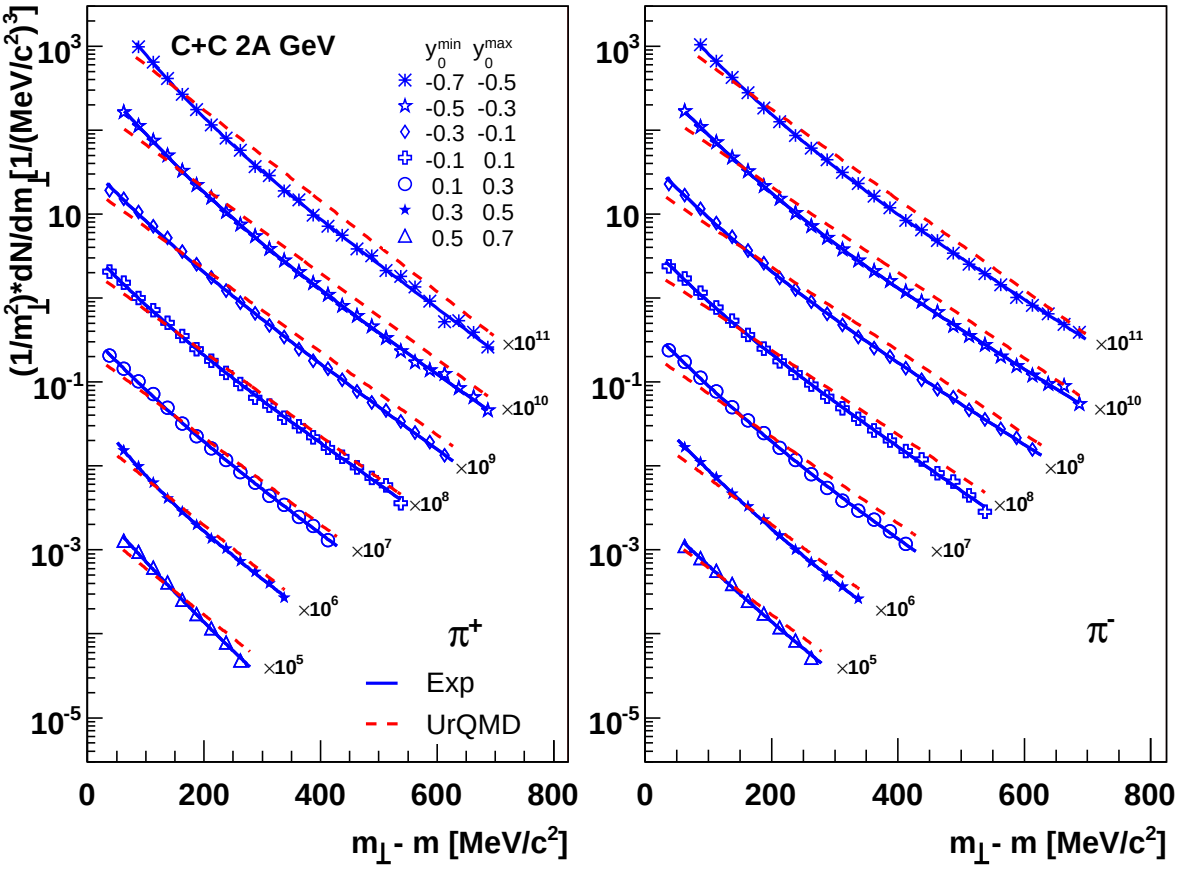

Fig. 9. Transverse-mass distributions for positively (left) and negatively (right) charged pions in different slices of rapidity derived from the data in ^{12}C + ^{12}C collisions at 2A GeV (LVL1 "semicentral" events). Full lines show the results of fits to the data (symbols) using two exponential functions, while dashed lines show fits of the UrQMD distributions using one exponential function. Error bars (systematic and statistical ones) are not visible at this scale. Both data and UrQMD distributions are normalized to the number of LVL1 events.

It is apparent that the yields and spectral shapes measured by all three experiments are in general fairly similar. The differences between integrated yields are within errors and do not exceed 10%. Looking at Fig. 10 in more detail, one sees that the measured charged-pion data agree for both bombarding energies (lower two plots, see insets for data ratios) over a large momentum range within errors (dominated by large systematic errors of the KaoS data). On the contrary, the comparison of charged and neutral π mesons (upper 4 plots) shows significant deviations for both beam energies, most apparent in the 2A GeV case (see inset of the upper right plot). As a consequence, our data on charged pions can be described only by a two-slope fit, while the TAPS π^0 data at this energy need only a single-exponential fit [27]. This may indicate differences in the reaction dynamics of charged and neutral π mesons, not present in transport codes. It is interesting to note that the pattern of the π^0/π^- ratio changes with beam energy as well (see insets in middle row in Fig. 10).

Other fits of our pion transverse-momentum distributions are in principle conceivable. For instance, a blast wave fit (see e.g. [28]) can be used. However, if applied to only one particle type it does not allow for an unambiguous determination of the flow parameter.

4.2 Rapidity distributions

As seen in the previous section, the HADES acceptance in transverse momentum is rather large. For the missing parts of the acceptance at low and high $p_\perp$ we extrapolated the pion yield. In doing so, for each slice centered at rapidity y the corresponding $p_\perp$ distribution was fitted with the function

$$\frac{1}{p_\perp^2}\frac{dN}{dp_\perp} = c_1(y)\exp\left(-\frac{p_\perp}{T_1(y)}\right) + c_2(y)\exp\left(-\frac{p_\perp}{T_2(y)}\right). \quad (3)$$

The fit results were then used to integrate the $\pi^\pm$ yield outside the acceptance. The resulting correction was $\approx 5\%$ and $\approx 2\%$ for π^+ and π^- respectively, except for data at large rapidities, where the correction was 10 - 20%. Fig. 11 shows the rapidity distributions normalized to the number of LVL1 events obtained from the integration of the extrapolated $p_\perp$ spectra of π^+ and π^- from ^{12}C + ^{12}C

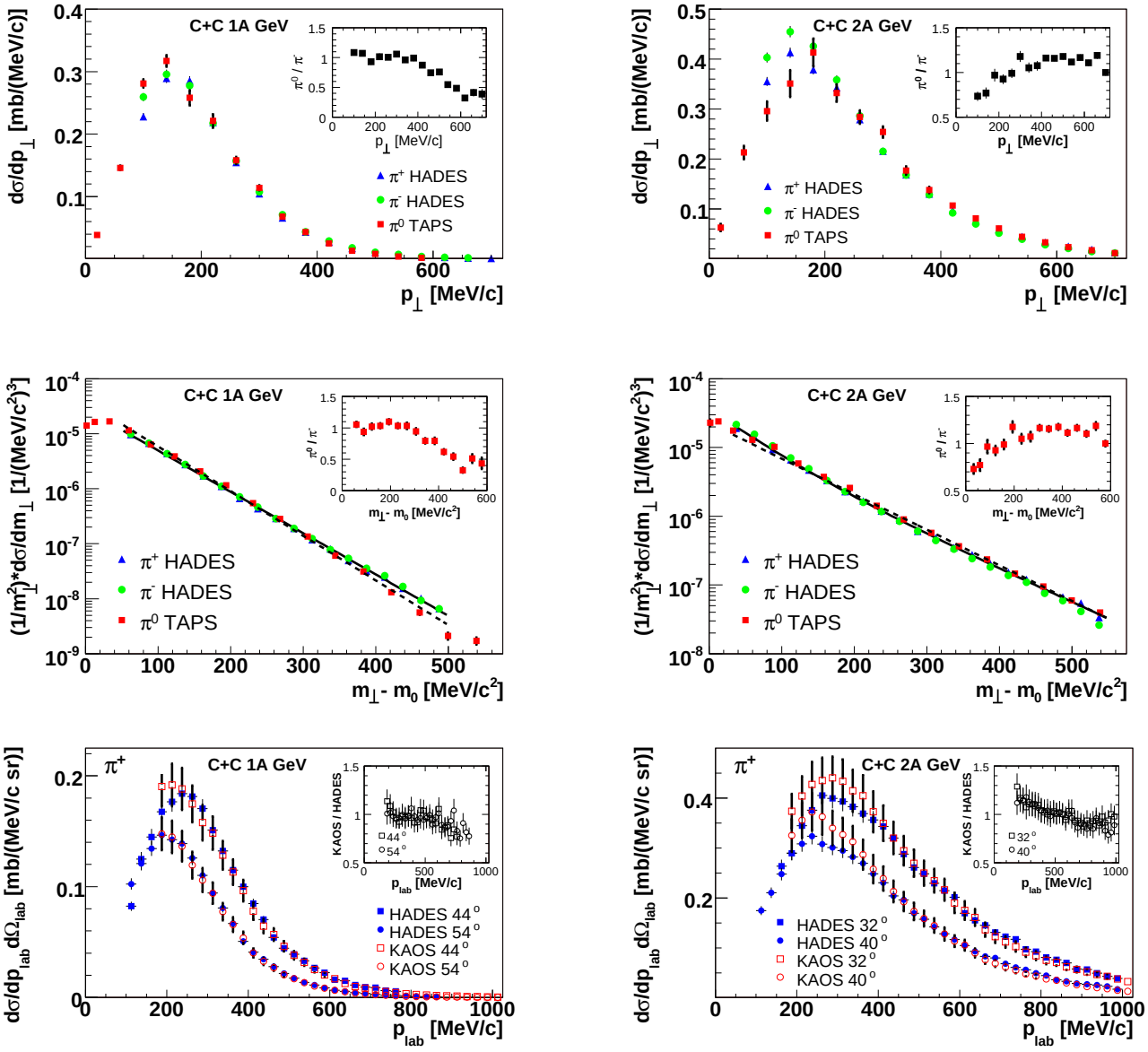

Fig. 10. Comparison of transverse-mass and transverse-momentum distributions of π mesons measured in the present experiment (HADES) and the previous TAPS [27] and KaoS [26] experiments. Top: Transverse-momentum ($p_\perp$) distributions of $\pi^{\pm,0}$ mesons for 1A GeV (left) and 2A GeV (right). Center: Transverse-mass ($m_\perp$) distributions of $\pi^{\pm,0}$ mesons for 1A GeV (left) and 2A GeV (right). Full lines show the results of fits of our data using two exponential functions, while dashed lines show fits of the TAPS π^0 distributions using one exponential function. Bottom: Momentum (p_{lab}) distributions of π^+ mesons for 1A GeV (left) and 2A GeV (right). The HADES data were rescaled to minimum-bias cross sections and filtered with the KaoS and TAPS acceptance filters (see text). Insets in all plots show the ratio of π yields on a linear scale.

at 1A GeV and 2A GeV. UrQMD simulation data (again normalized to the number of LVL1 events) are displayed as well. In order to extrapolate our data outside the accepted rapidity range, we used the Monte-Carlo event generator PLUTO described above. The simulation parameters - inverse slopes and anisotropies - were derived from our data, and the resulting rapidity distributions were normalized to the measured data.

The rapidity distributions exhibit a Gaussian-like shape with a standard deviation (σ referring to the scaled rapidity y_0) of about 1.0 for both beam energies. In the case of the 1A GeV data, the experimental rapidity distribution is about 20% narrower than the one from UrQMD. This is in agreement with the finding (see section 4.4 below) that the anisotropy parameter has a lower value in the experimental data than in UrQMD simulation. Note that

Table 2. Inverse slope parameters in units of MeV for $\pi^{\pm}$ measured at midrapidity derived from the data (using one and two exponential functions) and UrQMD (using one exponential function) in ^{12}C + ^{12}C collisions at 1 and 2A GeV.

Beam energy = 1A GeV				
Particle	Data		UrQMD	
	T (1 slope)	χ^2/ndf	T (1 slope)	χ^2/ndf
π^+	57.8 ± 0.3	1.7	55.4 ± 0.3	2.2
π^-	57.9 ± 0.3	1.4	55.4 ± 0.3	2.0

Beam energy = 2A GeV						
Particle	Data				UrQMD	
	T (2 slopes)	χ^2/ndf	T (1 slope)	χ^2/ndf	T (1 slope)	χ^2/ndf
π^+	47.7 ± 6.2; 90.6 ± 3.3	0.9	80.9 ± 0.5	4.7	86.5 ± 0.6	1.5
π^-	46.4 ± 5.2; 84.4 ± 2.1	1.2	76.7 ± 0.5	4.9	86.7 ± 0.6	1.4

for the 2A GeV case, a slight underestimation of our data by UrQMD is observed.

4.3 Multiplicities

Table 3. Particle yields per reaction (LVL1 trigger condition) of $\pi^{\pm}$ from ^{12}C + ^{12}C collisions. N_π and $N_\pi(4\pi)$ are the measured and 4π extrapolated yields, respectively. The statistical errors are negligible. Shown are the systematic errors due to the various efficiency corrections and to the 4π extrapolation (see text for details).

beam energy (A GeV)	particle	N_π	$N_\pi(4\pi)$
1	π^+	0.36±0.02	0.46±0.03±0.05
1	π^-	0.38±0.02	0.49±0.03±0.05
2	π^+	0.77±0.04	1.19±0.06±0.11
2	π^-	0.82±0.04	1.28±0.06±0.12

Pion yields (N_π) per reaction (under the LVL1 trigger condition) within the HADES acceptance region as shown in Fig. 11 and in full phase space are presented in Table 3. The systematic error of the measured yield due to uncertainties in the detection/reconstruction/identification efficiency is estimated as 5%, based again on a comparison of measurements in the six independent HADES sectors. The extrapolation of the yields to full phase space is based on the integration of the rapidity distributions simulated with PLUTO (see above) and normalized to the data in the rapidity range covered by HADES (see histograms in Fig. 11). Varying the input parameters of the PLUTO simulations - inverse slopes and angular anisotropy parameters - within their experimental errors, the differences between the rapidity distributions give us an estimate of the systematic error of the yield extrapolations of 9%.

Using the estimated averaged number of participants in the LVL1-triggered events (see in Table 1), the resulting $\pi^{\pm}$ multiplicity per participant (averaged for π^+ and π^-) is then $0.055 \pm 0.003 \pm 0.005 \pm 0.004$ and $0.147 \pm 0.007 \pm 0.013\ ^{+0}_{-0.021}$ at 1A GeV and 2A GeV, respectively. The three systematic errors of the yields correspond to uncertainties connected with the efficiency/purity corrections (5%), the extrapolation to full solid angle and full kinematic phase space (9%), and the determination of the number of participating nucleons (see Section 3.5).

Table 4 shows a comparison of measured π meson multiplicities per participant and results of our UrQMD simulations as well. The results agree within quoted errors.

Table 4. Comparison of multiplicities per participant of π mesons derived from our data with UrQMD results.

beam energy (A GeV)	particle	this work $\times 10^{-3}$	UrQMD $\times 10^{-3}$
1	$1/2(\pi^+ + \pi^-)$	$55 \pm 3 \pm 5 \pm 4$	59
1	π^0		67
2	$1/2(\pi^+ + \pi^-)$	$147 \pm 7 \pm 13\ ^{+0}_{-21}$	137
2	π^0		159

As we have shown above by comparing the momentum distributions, our results on integrated charged pion yields are consistent with the TAPS π^0 as well as the KaoS π^+ data. Due to experimental errors, it is however difficult to draw a conclusion on the difference in production yields of neutral and charged π mesons predicted by UrQMD (see Table 4).

4.4 Angular distributions

The measured centre-of-mass polar angular distributions of pions produced in 1A GeV and 2A GeV ^{12}C + ^{12}C collisions are exhibited in Fig. 12, together with the corresponding UrQMD distribution. Pions with centre-of-mass

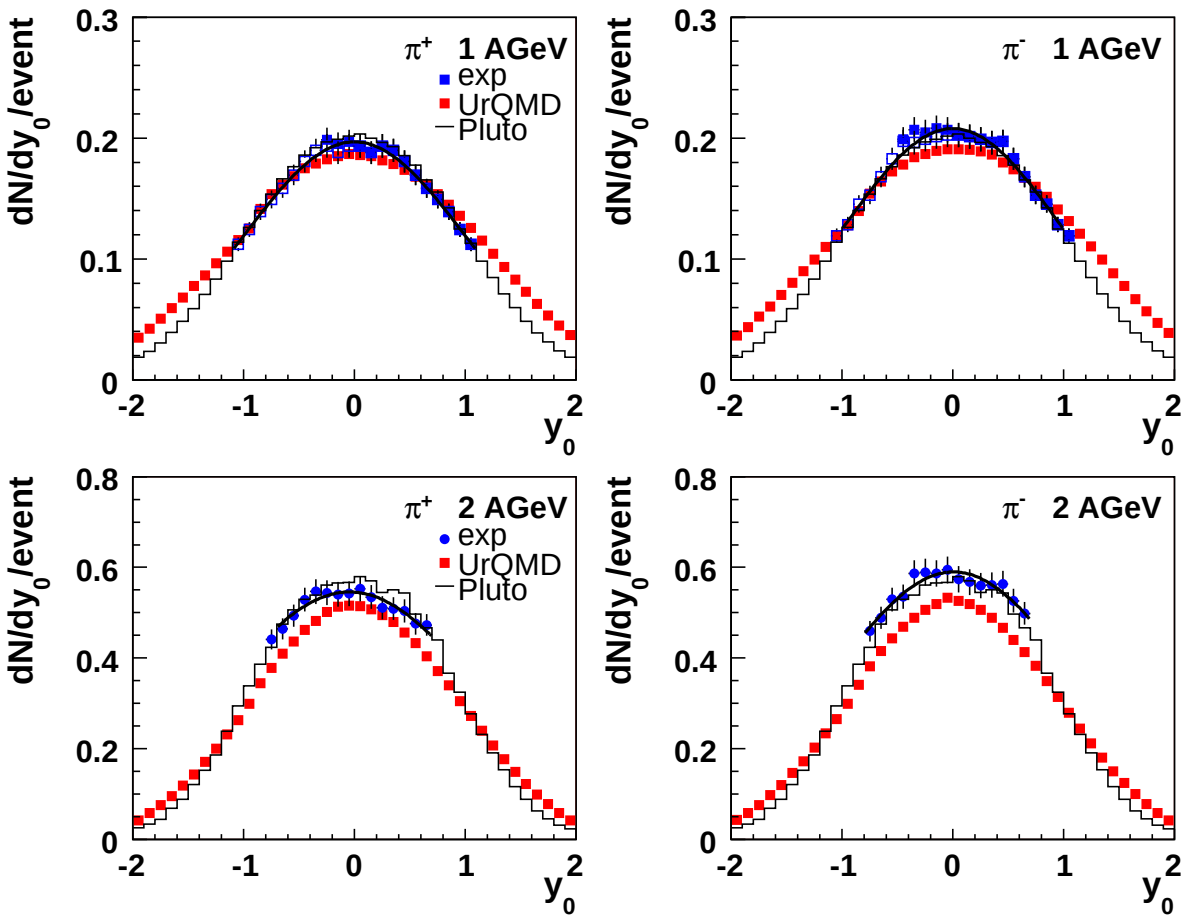

Fig. 11. The rapidity distribution of positively (left) and negatively (right) charged pions produced in ^{12}C + ^{12}C collisions at 1A GeV (top) and 2A GeV (bottom) for the LVL1 (semicentral) events. Circles with error bars show data, while full squares depict UrQMD calculations. The distributions obtained with the PLUTO generator are shown as histograms normalized to the measured yields (with π^+ and π^- averaged). In the 1A GeV case, the data points reflected from forward rapidities are shown as open symbols. The slight asymmetries of dN/dy with respect to reflection at $y_0 = 0$ are used to check the systematic errors.

momenta between 200 and 800 MeV/c have been selected. No losses in acceptance occur in this phase space region for the range of polar angles shown in Fig. 12. The systematic errors of the data are again estimated from the point-to-point differences between distributions from the six independent HADES sectors to be $\approx 5\%$ (see Sect. 3.5). As seen from the comparison of the measured data points and the ones reflected around 90° (see Fig. 12), this error underestimates the observed differences between the forward and backward hemisphere by a factor of < 1.5.

In the symmetric collision system ^{12}C + ^{12}C the polar distributions in the center-of-mass system can be fitted with the following expression

$$\frac{dN}{d(\cos\theta_{cms})} = A_1(1 + A_2\cos^2\theta_{cms}). \qquad (4)$$

The fit parameter A_2 characterizes the anisotropy of the pion source, and A_1 is a normalization. As visible in Fig. 12, the data show strong anisotropies quantified by $A_2 = 0.88 \pm 0.12$ and 1.19 ± 0.16 for beam energies of 1A GeV and 2A GeV, respectively. The UrQMD model gives similar anisotropies with $A_2 = 1.45$ and $A_2 = 1.12$ ($A_2 = 0.56$ and $A_2 = 0.70$ when integrated over all momenta, including also the region outside our acceptance).

We observe a strong dependence of the anisotropy on momentum. This is evident from Fig. 13, where A_2 is displayed as a function of the pion's centre-of-mass momentum from fits of Eq. (4) to our data. The data points for π^+ at highest displayed momenta are not shown, as they correspond to the phase space region (p_{lab} approaching 1000 MeV/c) where reliable particle identification becomes gradually impossible (see Fig. 3 in Sect. 3.3).

One can see that the anisotropy steadily increases with momentum for both pion charges and both beam energies up to $A_2 \simeq 1.0 - 1.5$, around 400 MeV/c, where it has a tendency to level off. This behavior is fairly well reproduced by the UrQMD model, which, however, tends to

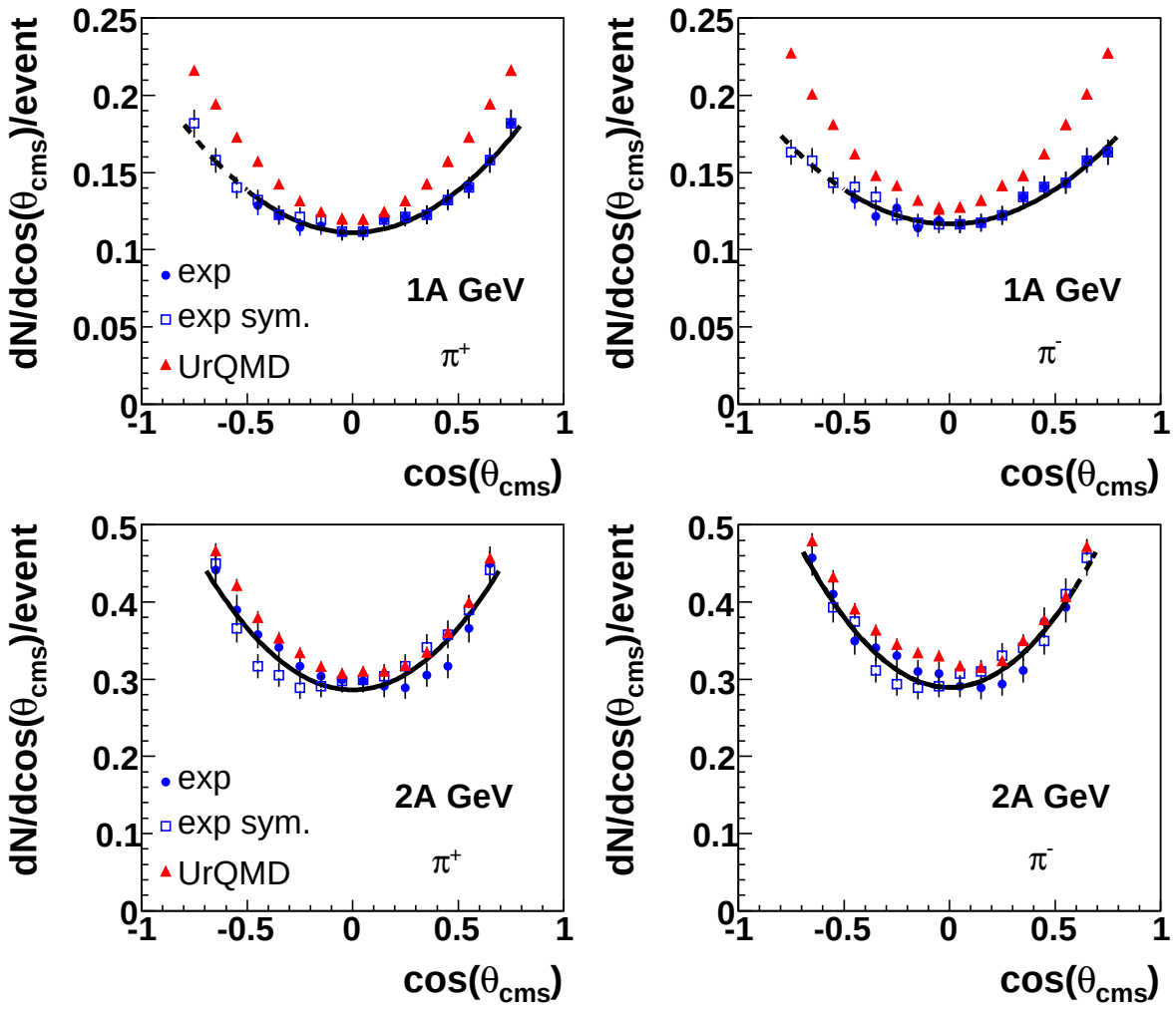

Fig. 12. Polar angle distribution in the center-of-mass system of positively (left) and negatively (right) charged π mesons produced in ^{12}C + ^{12}C collisions at 1A GeV (top) and 2A GeV (bottom) for the LVL1 (semicentral) events. Pions with center-of-mass momenta 200 - 800 MeV/c have been selected. Full circles show measured data. The data points reflected around 90° are shown as open squares. The full lines show the fit by Eq. (4), the extrapolations of the fits outside the acceptance are plotted as dashed lines. The UrQMD points are displayed as triangles, no fits to the UrQMD points are shown.

level off at somewhat larger values of the anisotropy in case of the 1A GeV data (see Fig. 13). For the data in the region 100 MeV/c $< p_{cms} <$ 200 MeV/c, the anisotropy can be fitted in a limited Θ_{cms} range only. The results show significantly lower A_2 parameters for both the data and UrQMD. The close-to-zero (at 2A GeV) and even slightly negative anisotropies given by UrQMD for low momenta at 1A GeV are not seen in the experiment.

It is interesting to compare these distributions to the corresponding ones of the elementary $NN \rightarrow N\Delta \rightarrow NN\pi$ reactions which are expected to be the dominant source of pion production at these beam energies [7,8]. In order to estimate the latter we have again used our PLUTO generator employing measured Δ distributions to model the proton-proton reaction [29]. We find that the shape of the simulated A_2 distributions is similar to the one found in ^{12}C + ^{12}C, but A_2 levels off at substantially higher values: namely 3.5 and 5 for 1A GeV and 2A GeV, respectively. The lower A_2 values found for ^{12}C + ^{12}C may be attributed to pion re-scattering and final state interactions even in the small system under consideration here.

Prior to the present work no data had been published on pion anisotropies in ^{12}C + ^{12}C collisions. Early studies of pion production in Ne-induced reactions at 0.8A GeV on NaF, Cu and Pb targets had found almost isotropic angular distributions for very low pion cms kinetic energies ($E_{\pi^+} \leq$ 50 MeV), but substantial anisotropies for all higher energies ($E_{\pi^+} \geq$ 150 MeV) [30]. The two closest systems studied most comprehensively in this respect are Ar+KCl at 0.8A GeV as well as 1.8A GeV [31,32] and Ca+Ca at 1.93A GeV [9]. While in both cases similar momentum-averaged anisotropies were observed, with values of $\langle A_2 \rangle = 0.5 - 0.6$, only the Ar+KCl data display

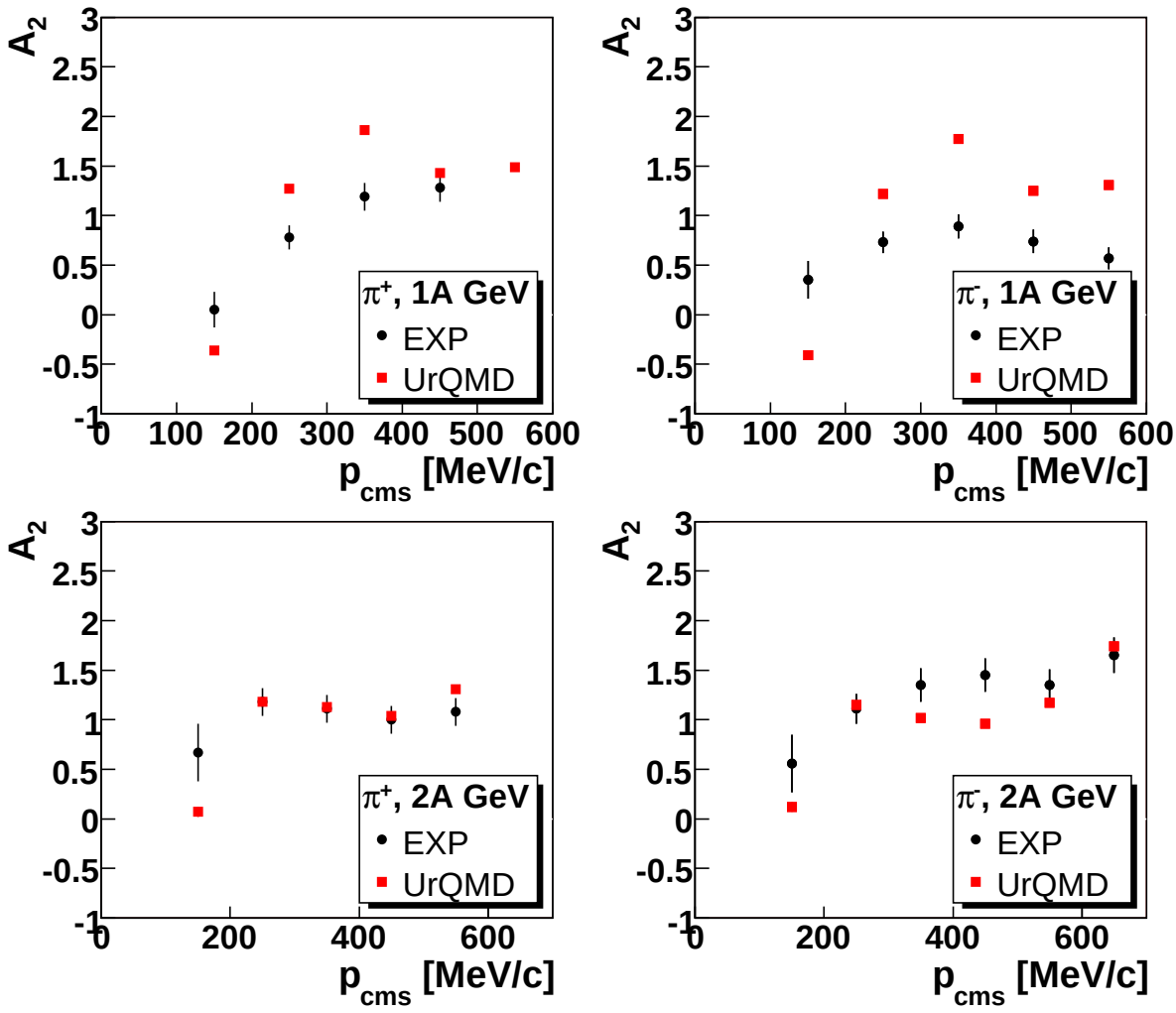

Fig. 13. Dependence of the anisotropy parameter A_2 on the momentum in the center-of-mass system for positively (left) and negatively (right) charged pions produced in ^{12}C + ^{12}C collisions at 1A GeV (top) and 2A GeV (bottom) for the LVL1 (semicentral) events. Circles with error bars show fits to the data, while squares exhibit fits to UrQMD simulations after they were subjected to the full analysis chain. Errors of the UrQMD points are smaller than the symbol size.

a strong pion-energy dependence of A_2, peaking around E_π = 200 - 300 MeV. Based on a comparison with transport calculations, the authors of Ref. [9] attributed these differences to the very different centralities covered by the two measurements. As seen from Fig. 13 and as discussed above, we do not observe in ^{12}C + ^{12}C, at both bombarding energies, a rise and fall of A_2, but rather a simple levelling-off with increasing pion cms momenta.

As the momentum dependence of A_2 has been claimed to depend strongly on the reaction centrality [9], we tried to study this effect in our data sample. First we checked, how the distribution differs in UrQMD events for the minimum-bias and LVL1-triggered events (see Sect. 3.4). The effect is negligible, as could be expected for a very weak preference of more central events of the LVL1 trigger in the light ^{12}C + ^{12}C system. Then we selected the 10% of "most central" events in the measured and UrQMD data samples by requiring more than 3 identified protons in the event. Again, we did not observe any significant difference with respect to the LVL1 data samples.

5 Summary

In summary, the charged-pion characteristics in the reaction ^{12}C + ^{12}C at 1A GeV and 2A GeV have been measured in detail with the HADES spectrometer. The found π meson yields are in good agreement with previous results obtained with the TAPS and KaoS detectors. The much larger acceptance of the present experiment, as compared to older measurements allowed for a more precise and reliable extrapolation of the yields to full solid angle, which is essential for the normalization of our dielectron yields in this reaction system.

Our data on the pion transverse-mass distributions at midrapidity can be described by a Maxwell-Boltzmann

function for 1A GeV, while the 2A GeV data show a strong second exponential component with smaller slope. This finding is in agreement with former results for the same system and energy for $\pi^{\pm}$ [26], whereas π^0 data [27] exhibit only a one-slope behaviour. The reasonable agreement of our transverse-momentum spectra at 1A GeV with UrQMD calculations indicates that the degree of thermalization in the light $^{12}C + ^{12}C$ system is adequately reproduced in this transport model. At 2A GeV, however, some deviations of our data from the UrQMD results become visible.

In contrast to the TAPS and KaoS data, which were measured in a limited angular range, strong pion anisotropies could be observed in the much larger acceptance region of the present experiment. The systematics [9] of pion production in heavier systems at comparable beam energies points to similar anisotropy values as extracted from our data sample. The asymmetries have a non-trivial momentum dependence. A peaking of the asymmetry as reported in [31], however, can not be confirmed. The comparison of our results with proton-proton data suggests that the angular anisotropies observed in $^{12}C + ^{12}C$ are remnants of the much stronger effect characteristic for inelastic nucleon-nucleon scattering.

Acknowledgments

The HADES collaboration gratefully acknowledges the support by BMBF grants 06MT238, 06TM970I, 06GI146I, 06F-140, 06FY171, and 06DR135, by DFG EClust 153 (Germany), by GSI (TM-KRUE, TM-FR1, GI/ME3, and OF/STR), by grants GA AS CR IAA100480803 and MSMT LC 07050 (Czech Republic), by grant KBN 5P03B 140 20 (Poland), by INFN (Italy), by CNRS/IN2P3 (France), by grants MCYT FPA2006-09154, XUGA PGID IT06PXIC296091PM and CPAN CSD2007-00042 (Spain), by grant FTC POCI/FP /81982 /2007 (Portugal), by grant UCY-10.3.11.12 (Cyprus), by INTAS grant 06-1000012-8861 and EU contract RII3-CT-2004-506078.

References

1. R. Stock, Phys. Rep. 135, 259 (1986).
2. P. Senger and H. Ströbele, J. Phys. G 25, R59 (1999).
3. W. Cassing and E. Bratkovskaya, Phys. Rep. 308, 65 (1999).
4. E. Bratkovskaya et al., Phys. Rev. C 69, 054907 (2004).
5. M. Wagner, A.B. Larionov, and U. Mosel, Phys. Rev. C 71, 034910 (2005).
6. V. Metag, Prog. Part. Nucl. Phys. 61, 245 (2008).
7. A.B. Larionov and U. Mosel, Nucl. Phys. A 728, 135 (2003);
   S. Teis et al., Z. Phys. A 356, 421 (1997).
8. A. Engel, A.K. Dutt-Mazumder, R. Shyam, and U. Mosel, Nucl. Phys. A 603, 387 (1996).
9. W. Reisdorf et al. (FOPI collaboration), Nucl. Phys. A 781, 459 (2007).
10. G. Agakishiev et al. (HADES collaboration), arXiv:0902.3478v1 [nucl-ex], to be published.
    R. Schicker et al. (HADES collaboration), Nucl. Instr. Meth. A 380, 586 (1996).
11. G. Agakishiev et al. (HADES collaboration), Phys. Rev. Lett. 98, 052302 (2007).
12. G. Agakishiev et al. (HADES collaboration), Phys. Lett. B 663, 43 (2008).
13. A. Balanda et al., Nucl. Instr. Meth. A 531, 445 (2004).
14. C. Agodi et al., Nucl. Instr. Meth. A 492, 14 (2002).
15. J. Lehnert at al., Nucl. Instr. Meth. A 502, 261 (2003).
16. A. Toia et al., Nucl. Instr. Meth. A 502, 270 (2003).
17. S.A. Bass et al., Prog. Part. Nucl. Phys. 41, 225 (1998).
18. M. Bleicher et al., J. Phys. G 25, 1859 (1999).
19. R. Brun et al., GEANT3 users guide, CERN-DD/EE/84-1 (1987).
20. I. Fröhlich et al. (HADES collaboration), arXiv:0708.2382 [nucl-ex].
21. W.H. Press, S.A. Teukolski, W.T. Vetterling, and B.P. Flannery, "Numerical Recipies", 4th edition, Cambridge University Press (2007).
22. A. Stuart and A.K. Ord, "Kendall's Advanced Theory of Statistics", Vol. I. Distribution Theory 5th Ed. (Oxford University Press, New York, 1987).
23. R. Barlow et al., *Recommended Statistical Procedures for BABAR*, BABAR analysis document No.318, (2002), www.slac.stanford.edu/BFROOT/www/Statistics/Report/report.pdf.
24. B. Hommez, Nucl. Instr. Meth. A 502, 294 (2003).
25. J. Gosset et al., Phys. Rev. C 16, 629 (1977);
    J. Hüfner and J. Knoll, Nucl. Phys. A 290, 460 (1977).
26. F. Laue et al. (KaoS Collaboration), Eur. Phys. J. A 9, 397 (2000);
    C. Sturm, PhD thesis, TU Darmstadt, 2001, http://elib.tu-darmstadt.de/diss/000166/.
27. R. Averbeck et al. (TAPS Collaboration), Z. Phys. A 359, 65 (1997).
28. K. Adcox et al. (PHENIX collaboration), Phys. Rev. C 69, 024904 (2004).
29. V. Dmitriev, O. Sushkov and C. Gaarde, Nucl. Phys. A 459, 503 (1986).
30. J. Chiba et al., Phys. Rev. C 20, 1332 (1979).
31. R. Brockman et al., Phys. Rev. Lett. 53, 2012 (1984).
32. S. Nagamiya et al., Phys. Rev. C 24, 971 (1981).